Clim Dyn (2013) 41:63–79
DOI 10.1007/s00382-012-1587-6

Observational climatology and characteristics of wintertime atmospheric blocking over Ural–Siberia

Ho Nam Cheung · Wen Zhou · Yaping Shao · Wen Chen · Hing Yim Mok · Man Chi Wu

Received: 14 June 2012 / Accepted: 3 November 2012 / Published online: 20 November 2012

Abstract This study investigates the climatological aspects and temporal characteristics of wintertime Ural-Siberian blocking (USB, centered over 30°–100°E), for the period 1980/1981–2009/2010. Sixty-eight events are identified and their physical structure is diagnosed using thermodynamic and geostrophic vorticity tendency equations. In climatology, horizontal advections play a fundamental role in constructing a USB event, in which the anticyclonic center is a warm core in the troposphere and a cold core in the lower stratosphere. The decay of the thermal structure is related to diabatic cooling along the vertical structure and warm advection in the lower stratosphere. Meanwhile, the collapse of the height structure is caused primarily by cyclonic vorticity advection. A strong interrelationship exists between the intensity and extension of USB events. The temporal characteristics of USB events are analyzed by examining strong and weak events, which are of high and low intensity. The strong events are probably preceded by an open ridge over Europe and a cyclogenesis over the Mediterranean Sea, and their formation is followed by the stronger amplification of a Rossby wave packet across Eurasia. On the other hand, the weak events are likely to be triggered by surface cold anomalies over Siberia. Overall, the evolution of a USB event forms a dynamic linkage with the Siberian high, in which the decay stage of the USB event is accompanied by a southeastward migration of the Siberian high and a subsequent cold air outbreak in East Asia. These results advance our understanding of USB and its relationship with East Asian winter monsoon activities.

Keywords Atmospheric blocking · Climatology · Diagnostic analysis · Ural Mountains · Wintertime circulation

H. N. Cheung · W. Zhou
Shenzhen Research Institute, City University of Hong Kong, Shenzhen, China

H. N. Cheung · W. Zhou (✉)
Guy Carpenter Asia–Pacific Climate Impact Centre, School of Energy and Environment, City University of Hong Kong, Kowloon, Hong Kong, China
e-mail: wenzhou@cityu.edu.hk

Y. Shao
Institute for Geophysics and Meteorology, University of Cologne, Cologne, Germany

W. Chen
Center for Monsoon System Research, Institute of Atmospheric Physics, Chinese Academy of Sciences, Beijing, China

H. Y. Mok · M. C. Wu
Hong Kong Observatory, Hong Kong, China

1 Introduction

Atmospheric blocking describes a large-scale anticyclone that remains quasi-stationary over the extratropics longer than synoptic timescales. The persistence of blocking often exerts a high impact upstream and downstream, and therefore blocking is a critical challenge in short-term and medium-range weather forecasts (e.g., Shabbar et al. 2001; Trigo et al. 2004). Over the Northern Hemisphere, the climatology of blocking frequency reaches two peaks over the Euro-Atlantic region and the Pacific Ocean (e.g., Tibaldi and Molteni 1990; Barriopedro et al. 2006). In addition, blocking sometimes occurs independently in the vicinity of the Ural Mountains (~60°E; Diao et al. 2006); this is called Ural-Siberian blocking (USB, 30°–100°E) in

this study (Cheung et al. 2012a). While previous studies have thoroughly documented the climatology of blocking frequency in different seasons (e.g., Barriopedro et al. 2006; Diao et al. 2006; Croci-Maspoli et al. 2007; Tyrlis and Hoskins 2008a; Cheung et al. 2012b), there are few climatological studies on the energetics and dynamics of blocking events (Nakamura et al. 1997; Takaya and Nakamura 2005b; Tyrlis and Hoskins 2008b).

During boreal winter, blocking is generally more active, more intense, and more extensive (Lupo and Smith 1995a; Barriopedro et al. 2006; Cheung et al. 2012b). In particular, USB has been found to exert a considerable impact on East Asian winter monsoon (EAWM) activities (Wu and Leung 2009; Wang et al. 2010; Cheung et al. 2012a, b; Chang and Lu 2012). Because the persistence of USB enhances the cold advection downstream that reinforces the Siberian high, USB has been identified as an important precursor of severe cold surges in East Asia (Tao 1957; Joung and Hitchman 1982; Takaya and Nakamura 2005a, b; Lu and Chang 2009). In January 2008, the recurrence of USB helped maintain a cold downstream background that allowed an unusually long-lasting and severe snowstorm to take place in southern China (Tao and Wei 2008; Zhou et al. 2009; Li and Gu 2010). However, Wang et al. (2010) noticed that wintertime USB activity has undergone a remarkable decline in the past few decades. In association with weaker USB activity, more planetary waves were found to propagate equatorward in the troposphere instead of propagating upward toward the stratosphere, which is similar to the wave activities in weak EAWM years as described by Chen et al. (2005) and Chen and Li (2007). Thus, the weakened USB activity is likely responsible for the weakening intensity of the winter-mean Siberian high and the EAWM in recent decades. Although substantial evidence has shown how USB may be dynamically linked to the East Asian winter climate on seasonal timescales, the climatology of USB frequency is only around 5 days [see Fig. 1 in Cheung et al. (2012b)]. Accordingly, we are of great concern for analyzing the impact, as well as the energetics and dynamics, of USB events of differing intensity and extension.

Blocking formation is often preceded by an explosive surface cyclogenesis (e.g., Colucci 1985; Tsou and Smith 1990). This precursor explains why the two peaks of climatological blocking frequency are located in the exit region of the climatological storm track over the two ocean basins. The cyclone advects warm and anticyclonic vorticity eddies poleward. Diagnostic studies have shown that anticyclonic vorticity advection plays a crucial role in blocking formation (Tracton 1990; Alberta et al. 1991) as well as its maintenance (Mullen 1987). During the early stage of blocking development, the anticyclonic eddy flux leads the developing blocking high by nearly one-quarter of a wavelength (Illari 1984; Mullen 1987). Then, the blocking high develops rapidly as its anticyclonic vorticity is increased by the incoming high-frequency eddies (Holopainen and Fortelius 1987). Its maintenance is supported by barotropic forcing, whereas the baroclinic eddy flux decays (Alberta et al. 1991; Nakamura and Wallace 1993). Nakamura et al. (1997) analyzed strong blocking events over Europe and the Pacific and found that the interaction with quasi-stationary Rossby waves plays a more important role in the blocking formation over Europe. Meanwhile, the transient eddy forcing is crucial over the Pacific, but it also determines the intensity of blocking in Europe.

Recently, Takaya and Nakamura (2005b) suggested that the blocking formation over Eurasia can be attributed primarily to the interaction between the Siberian high and the eastward-propagating Rossby wavetrain. While blocking moves eastward over western Siberia, it enhances the surface northerly cold advection on the northwestern flank of the Tibetan Plateau. This is crucial for amplifying the Siberian high before a cold air outbreak. Indeed, such an eastward-propagating wavetrain has been regarded as a major teleconnection pathway (Joung and Hitchman 1982; Blackmon et al. 1984; Pan 1987; Chan and Li 2004). It exhibits a barotropic structure over Europe, but it slows down and moves southeastward over central and western Siberia with increasing baroclinicity. The difference in blocking is due to the modest feedback exerted by the surface. If there are preexisting surface cold anomalies, the cold air also induces a cyclonic anomaly over Ural–Siberia and an anticyclonic anomaly upstream in the upper troposphere. Consequently, this sector blocking stays quasi-stationary and interacts with the Siberian high (Takaya and Nakamura 2005a).

Even though considerable effort has been made to study the energetics and dynamics of blocking using case studies, there is still not a complete climatology of this issue regarding the evolution of USB. In addition, there are no analyses of the physical mechanisms of USB events with different temporal characteristics, such as intensity and extension. These two aspects are vital for understanding the relationship between USB and EAWM activities and are therefore the focus of this study. Throughout this study, we attempt to address the following questions: (1) What are the major physical mechanisms for the development and decay of USB from the climatological point of view? (2) Are there any differences in the energetics and dynamics of characteristic USB events? (3) What are the consequences of these characteristic events on EAWM activities?

This paper is organized as follows: Sect. 2 describes the data and methods. Then, Sect. 3 presents the climatology of wintertime USB, including its 3-dimensional structures and its linkage with the Siberian high. Section 4 further analyzes the characteristics of blocking events, including both strong and weak events. The results are summarized and discussed in Sect. 5.

2 Data and methods

2.1 Data

We use daily fields of the NCEP-NCAR reanalysis datasets with a spatial resolution of 2.5° latitude × 2.5° longitude at the $\sigma_{99.5}$ level (surface) and 17 pressure levels (1,000, 925, 850, 700, 600, 500, 400, 300, 250, 200, 150, 100, 70, 50, 30, 20 and 10 hPa) for the period 1980/1981–2009/2010 (Kalnay et al. 1996). The surface parameters include air temperature (T; i.e., surface air temperature, SAT), sea level pressure (SLP), and the zonal and meridional components of vector wind (U and V). In addition to T, U, and V, the multiple-level parameters include omega (W; available from 1,000 to 100 hPa) and geopotential height (Z).

The winter of each year includes the five consecutive months from November through March (NDJFM), where the year denotes the beginning month of that winter. Moreover, an anomaly on a given calendar day, unless specified otherwise, is defined as a departure from its daily climatology, which is obtained from the 11-day running mean over the 30-year study period. The significance level for comparing two samples is determined by the two-tailed Student's *t* test.

2.2 Detection of atmospheric blocking

The detection of blocking events and the definition of their characteristics principally follows the procedures outlined in Barriopedro et al. (2006). A brief description of the algorithm is provided here. All blocking regions are defined by the daily field of the 500 hPa geopotential height (Z500). Each region is composed of at least five consecutive longitude grid points (i.e., extension ≥12.5° longitude) that satisfy the three sets of equations in (1) for at least 1 of 5 latitude grid point pairs (ϕ_N, ϕ_0, ϕ_S). The first two equations are to measure the meridional gradients of Z500 over the extratropical regions (ZGN, ZGS) to determine whether a longitude grid point (λ) belongs to the blocking-type circulation. Meanwhile, the third criterion is to ensure that the central part of the region is an anticyclone, where a bar over Z500 denotes the daily climatology.

$$\begin{aligned}
&\mathrm{ZGN}(\lambda) = \frac{Z(\lambda,\phi_N) - Z(\lambda,\phi_0)}{\phi_N - \phi_0} < -10\,\mathrm{m/deglat}\\
&\mathrm{ZGS}(\lambda) = \frac{Z(\lambda,\phi_0) - Z(\lambda,\phi_S)}{\phi_0 - \phi_S} > 0\\
&\mathrm{Z500}(\lambda,\phi_0) - \overline{\mathrm{Z500}(\lambda,\phi_0)} > 0
\end{aligned} \tag{1}$$

where $\lambda \in [0, 357.5]^{\circ}E$, $\phi_N = 80^{\circ}\mathrm{N} + \Delta$, $\phi_0 = 60^{\circ}\mathrm{N} + \Delta$, $\phi_S = 40^{\circ}\mathrm{N} + \Delta$, $\Delta = -5^{\circ}, -2.5^{\circ}, 0^{\circ}, 2.5^{\circ}$, or 5° latitude.

The extension of a blocking region is taken as the distance between the easternmost and westernmost longitude grid point. The center (λ_{ctr}, ϕ_{ctr}) corresponds to the grid point of the largest zonally averaged and meridionally averaged Z500 within a reference region. This reference region is extended 5° longitude eastward and westward from the easternmost and westernmost grid point, respectively, concerning the tilting of some blocking ridges. After identifying the center, the intensity of a blocking region is determined by Eq. (2), in which λ_{up} and λ_{down} represent the upstream and downstream longitude grid points at the half extension from λ_{ctr} of that blocking region.

$$\begin{aligned}
&\mathrm{BI} = 100.0[Z(\lambda_{ctr},\phi_{ctr})/Z_{ref} - 1.0],\\
&\text{where } Z_{ref} = \left[Z\left(\lambda_{up},\phi\right) + Z(\lambda_{down},\phi)\right]/2
\end{aligned} \tag{2}$$

2.3 Diagnostic equations

The thermal and height structures of USB are diagnosed by the thermodynamic energy equation and the vorticity tendency equation, respectively, in isobaric coordinates (λ, ϕ, p; Holton 1979; Lupo et al. 1992). First, at a given pressure level (p), the thermodynamic energy equation, or the temperature tendency equation, is written as

$$\frac{\partial T}{\partial t} = \underbrace{-\left(U\frac{\partial T}{\partial \lambda} + V\frac{\partial T}{\partial \phi}\right)}_{b} \underbrace{-W\frac{T}{\theta}\frac{\partial \theta}{\partial p}}_{c} \underbrace{+\frac{\dot{Q}}{C_P}}_{d} \tag{3}$$

where the terms on the R.H.S. are (*b*) the horizontal temperature advection, (*c*) an adiabatic heating term due to vertical motion and (*d*) diabatic heating. For the diabatic heating term, $\dot{Q}$ is the diabatic heating rate per unit mass, and c_p is the specific heat at constant pressure (=1,004 J K^{-1} kg^{-1}). In this study, this term is approximated as the residual of the other three terms in the equation. T, U, V, and W are extracted from the NCEP-NCAR reanalysis datasets, whereas θ, the potential temperature, is derived from T using Poisson's equation.

Second, the geostrophic vorticity tendency equation at a specific pressure level is expressed as:

$$\underbrace{\frac{\partial \xi_g}{\partial t}}_{e} = \underbrace{-\frac{1}{a}\left(U\frac{\partial \xi_a}{\cos\phi\partial\lambda} + V\frac{\partial \xi_a}{\partial\phi}\right)}_{f} \underbrace{-\frac{\xi_a}{a}\left(\frac{\partial U}{\cos\phi\partial\lambda} + \frac{\partial V}{\partial\phi}\right)}_{g} \underbrace{-\frac{1}{a}\left(\frac{\partial W}{\cos\phi\partial\lambda}\frac{\partial V}{\partial p} - \frac{\partial W}{\partial\phi}\frac{\partial U}{\partial p}\right)}_{h} \underbrace{-W\frac{\partial \xi_a}{\partial p}}_{i} \underbrace{+\frac{1}{a}\left(\frac{\partial F}{\partial\phi} - \frac{\partial F}{\cos\phi\partial\lambda}\right)}_{j} \underbrace{-\frac{\partial \xi_{ag}}{\partial t}}_{k} \quad (4)$$

where the terms on the R.H.S. are (f) the horizontal vorticity advection, (g) the divergent effect, (h) the tilting effect, (i) the vertical vorticity advection, (j) the frictional effect, and (k) the ageostrophic vorticity tendency. ξ indicates the vorticity, and the subscripts a, g, and ag attached to this quantity denote absolute, geostrophic, and ageostrophic vorticity, respectively. The quantity a in the reciprocal of terms f, g, h, and j denotes the earth's radius.

In the above equations, the partial derivatives in the λ, ϕ, and p directions are determined by the 2nd-order centered finite difference method, except that the boundaries of ϕ (90°N and 90°S) and p (1,000 and 10, or 100 hPa for W) use the one-sided finite difference method. Note that the effect of frictional force (term j) is generally small and is not taken into consideration in our analyses.

3 A climatology of wintertime Ural-Siberian blocking (USB)

All USB events in this study are centered between 30° and 100°E longitude when they are established (Cheung et al. 2012a). For a wintertime event, the establishment date falls between 1 November and 31 March and the duration is at least 4 days. During the period 1980–2009, 68 USB events are identified and their mean center is located at 64.3°N, 58.3°E. The statistics of the temporal characteristics of these events, including duration, intensity, and extension, are summarized in Table 1. Among these events, however, the duration varies from 4 to 16 days and the center spreads across a considerable distance between 30° and 100°E. In order to acquire coherent signals for studying their physical structures during the development and decay stages, day 0 of each event is defined as the date that the event attained a maximum intensity. In addition, all physical parameters at the center on day 0 of each event are first translated to a reference grid (65.0°N, 57.5°E), which is the closest grid to the mean location under the 2.5° × 2.5° resolution of reanalysis datasets. Such a translation is then applied to other days of the same event. The center of a USB event is defined as spanning 5° across the reference grid (60°–70°N, 52.5°–62.5°E).

3.1 Physical structure

Figure 1 shows the climatology of thermal and height structures across the USB center. The vertical profiles in Fig. 1a–b illustrate the structure of a typical blocking high. The thermal structure is composed of a warm core in the troposphere and a cold core in the lower stratosphere (Fig. 1a). During the development stage, the high center acquires instability due to an increase in the vertical temperature gradient, and it is most pronounced near the tropopause (Fig. 1b). Moreover, Fig. 1c depicts the horizontal structure on day 0 by compositing Z500 and the thickness air temperature anomalies in the 1,000–300 hPa layer. On one hand, the height structure shows an omega-like pattern with a closed isopleth at 5,580 m, indicating the mature phase of the blocking high. On the other hand, the thermal structure is made up of a dipole anomaly pattern oriented in the NW–SE direction in the troposphere. As deduced by the mean extension from Table 1, the western and eastern ends of the USB are located near 40°E and 75°E, respectively. Accordingly, these results suggest that wintertime USB generally exerts a high impact downstream (i.e., western Siberia), which involves interaction between the quasi-stationary Rossby wave packet and the Siberian high, according to the findings of Takaya and Nakamura (2005a).

Table 1 Statistics of the intensity, extension, and duration of wintertime USB events

	Percentile (-th)					Mean	SD
	0	25	50	75	100		
Intensity (no unit)	0.9	3.0	4.3	5.6	10.1	4.3	1.8
Extension (km)	844	1,200	1,660	2,060	5,140	1,730	833
Duration (days)	4	4	5	7	16	6	3

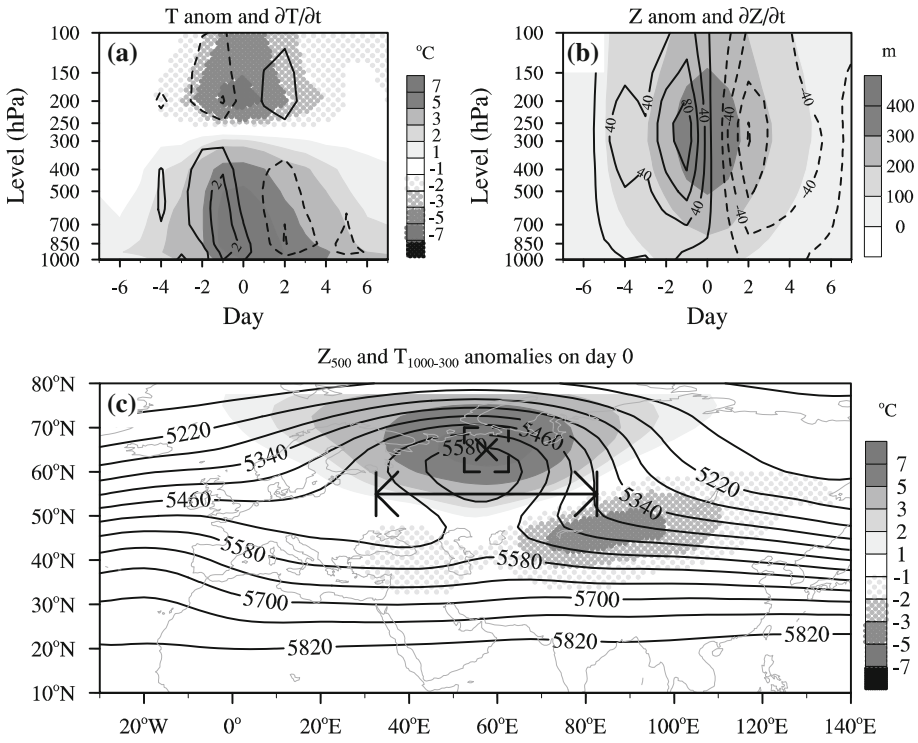

Fig. 1 Climatological structure of wintertime USB events. The *vertical* profiles of **a** temperature (unit: °C) and **b** height (unit: m) across their centers, where the contours and *shading* indicate the tendencies and anomalies. For the tendency term, the *solid* (*dashed*) contours represent positive (*negative*) values and the zero contours are omitted, where the unit is °C day^{-1} in (**a**) and m day^{-1} in (**b**). **c** A composite map on day 0: geopotential height at 500 hPa (contours; unit: m) and thickness air temperature anomalies in the 1,000–300 hPa layer (shading; unit: °C). In (c), the cross indicates the mean center, the *square box* encloses the central region of the blocking high, and the *arrow line* represents the median of the extension given by Table 1

The vertical structures across the USB center are analyzed using diagnostic equations (Eqs. 2–3), as mentioned in Sect. 2.3 (Figs. 2, 3). In climatology, USB develops between day −3 and 0 and it decays between day 1 and 4. In comparison, the decay rate is slower than the development rate (Figs. 2a, 3a), which may in turn indicate that intensification is a more abrupt procedure. Among all thermodynamic terms, the horizontal advection acts as the primary factor for USB formation, which is positive (negative) in sign in the troposphere (lower stratosphere; Fig. 2b). Furthermore, diabatic heating may play a secondary role in the warm-core structure in the midtroposphere (Fig. 2d). After development, the high stability in the middle and upper troposphere acquired by the blocking center gives rise to strong adiabatic warming (Fig. 2c). However, this is compensated by strong diabatic cooling in the troposphere (Fig. 2d). Meanwhile, the horizontal advection term is negligibly small in the troposphere but it is considerably positive in the lower stratosphere (Fig. 2a). Hence, the warm advection in the lower stratosphere and the diabatic cooling in the troposphere are two weakening processes that destroy the thermal structure.

On the other hand, the development and decay of the vorticity structure is attributable mainly to the horizontal advection of absolute vorticity, where the forcing is strongest near 300 hPa (Fig. 3a–b). During the development stage, part of the incoming anticyclonic vorticity advection counteracts the ageostrophic tendency and the divergence effect (Fig. 3d–e). The vertical advection of absolute vorticity seems to be negligibly small throughout the entire air column (Fig. 3f). The tilting term is generally small, but it may make a positive contribution to the development of blocking in the midtroposphere (Fig. 3c). The sign of each term obtained in the vorticity tendency equation is consistent with the findings of Lupo and Smith (1995b), who performed a diagnostic analysis on Atlantic blocking using the geopotential height tendency equation. During the decay stage, the horizontal vorticity advection is opposite in sign to most of the other terms, but it is the dominant factor.

3.2 Life cycle

The life cycle of a USB event is further investigated by the composites on day −2, day 0, and day 2 at three pressure levels (200, 500 hPa, and near-surface). The composites are given in Figs. 4, 5, 6, which illustrate thermodynamic and dynamic forcing, as well as thermal and height structures, across a USB event.

On day −2, the Icelandic low weakens substantially associated with a southeastward extension (Fig. 4f). There is an anomalous low over the Mediterranean Sea that is subject to intensification, which can be deduced by the negative SLP tendency over 20°E, 40°N (Fig. 4f). Downstream of this low anomaly is a thermal ridge extending northeastward to advect warm air toward the northwestern flank of the Siberian high (Fig. 4c). An upper-tropospheric height ridge lags behind the surface ridge (Fig. 4b–c),

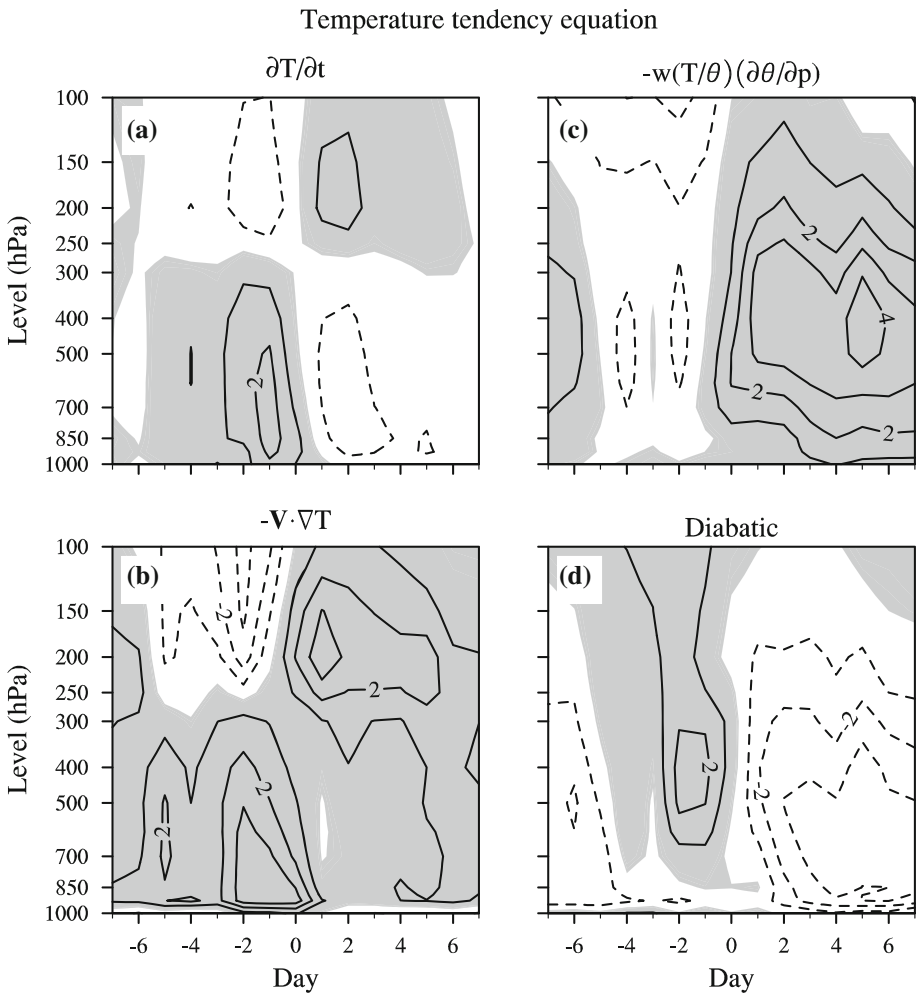

Fig. 2 *Vertical* profiles of individual terms in the temperature equations across the USB center: **a** temperature tendency, **b** *horizontal* temperature advection, **c** adiabatic heating, and **d** diabatic heating. Positive values are *shaded* and represented by *solid contours*, while negative values are represented by *dashed contours* and the zero contours are omitted. Contour interval: 1 °C day^{-1}

which resembles the typical structure of a developing baroclinic wave (Holton 1979). Accordingly, both the thermal and height ridges amplify and move slowly eastward. In addition, there is a thermal trough downstream of the warm ridge (Fig. 4b–c). Such a trough over the upper troposphere was found to increase the mass convergence and enhance the surface divergence over western Siberia prior to a cold air outbreak (Ding 1990; Wu and Chan 1997). The development of the Siberian high is signified by a sharp increase in the SLP and a substantial decrease in the SAT to the west of Lake Baikal (~50°N, 110°E; Fig. 4f). These results suggest that the Siberian high undergoes intensification during the development of USB.

The mature phase of a USB event is characterized by an omega-like height pattern over the upper troposphere on day 0 (Figs. 1b, 5b), although both thermodynamic and dynamic forcing are weaker than on day −2 (Figs. 4, 5). On day −2, the USB is centered at 60°N, 45°E (Fig. 4b), which almost coincides with the local maximum of height and SLP tendencies (Fig. 4d–f). This position also shows the greatest magnitude in temperature tendency in the upper air (Fig. 4d–e). Such baroclinic forcing favors substantial intensification of the USB. Comparatively, the tendencies lessen on day 0 (Fig. 5d–f), especially the positive SLP tendency over western Siberia (Fig. 5f). Moreover, the local maximum of these terms is located to the east of the USB center (65°N, 57.5°E), where the thermodynamic term is moved farther east than the dynamic term (Fig. 5d–f). The amplified thermal ridge extends farther northeastward, which enhances the pronounced warming across the northern flank of the USB (Fig. 5b–c). Consequently, the trough above the Siberian high intensifies the cooling near the surface. On the other hand, the SLP over the Icelandic low continues to increase, while the low anomaly over the Mediterranean Sea remains unchanged (Fig. 5f). Meanwhile, the zero-degree isotherm along the anomalous low remains quasi-stationary between day −2 and day 0 (Figs. 4c, 5c). Apparently, the upstream environment over the Euro-Atlantic region on day 0 does not exert a strong enough physical forcing to further intensify the USB.

On day 2, the USB weakens substantially and its center at 500 hPa loses the identity of the closed isopleth at

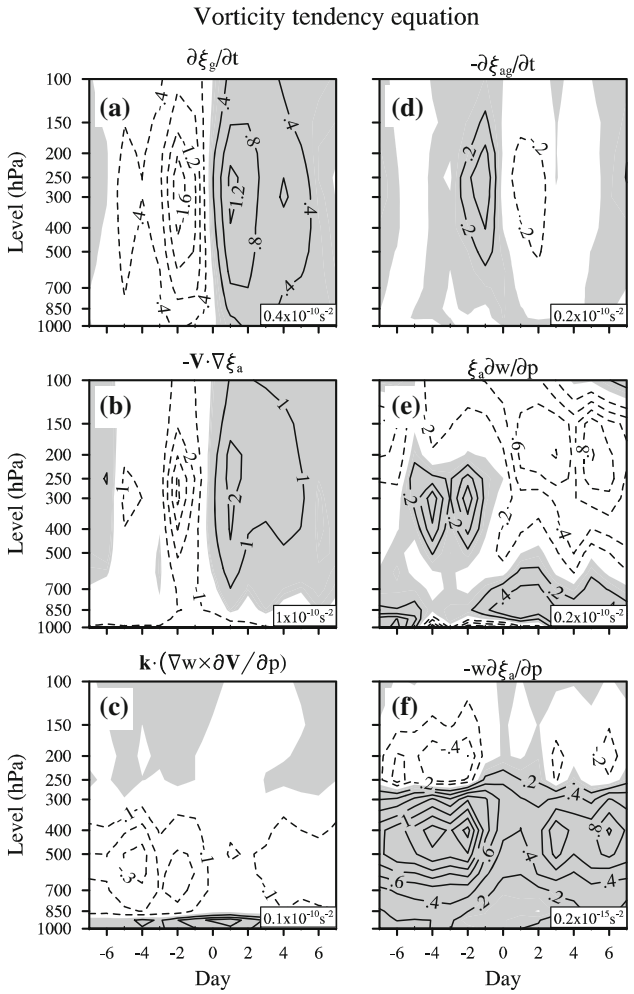

Fig. 3 *Vertical* profiles of individual terms in the geostrophic vorticity equation: **a** tendency of geostrophic vorticity, **b** *horizontal* advection of absolute vorticity, **c** tilting, **d** tendency of ageostrophic vorticity, **e** divergence term, and **f** *vertical* advection of absolute vorticity. The contour interval is shown at the *bottom right*, where the zero contours are omitted, positive values are *shaded*, and negative values are represented by *dashed lines*. Note that the contour interval ranges between 0.1×10^{-10} s^{-2} and 1×10^{-10} s^{-2} in (**a**–**e**) and it is set at 0.2×10^{-15} s^{-2} in (**f**)

5,580 m in the mature phase (Fig. 6b). The pressure and temperature tendencies coincide with the USB center again, but they are opposite in sign to those on day −2, suggesting that the weakening force is baroclinic. In the meantime the weakening signal transmits across East Asia, where the upper-tropospheric trough above the Siberian high exhibits positive pressure and temperature tendencies (Fig. 6e). This is associated with the breakdown of the Siberian high, which migrates southeastward by bringing cold air masses toward the East Asian continent. The positive SLP tendency, together with the negative temperature tendency to the southwest of Lake Baikal, indicates such a cold air outbreak (Fig. 6f). This is what previous studies have described as the occurrence of a severe cold surge following the collapse of a blocking ridge in the vicinity of the Ural Mountains (e.g., Tao 1957; Takaya and Nakamura 2005b). Overall, it appears that the evolution of a winter USB event is related to that of the Siberian high in climatology.

3.3 Relationship with the Siberian high

To further study the climatological linkage between USB and the Siberian high, the temporal variation of the two systems during the evolution of USB is analyzed by the geopotential height spanning 5° across the USB center, as well as the SLP and SAT over the Siberian high region. The Siberian high region is defined as 45°–55°N, 70°–90°E on the transformed grid, where the cold dome can be identified on day 0 (Fig. 1c). This region is located to the west of the climatological Siberian high region for studying cold surges [e.g., 40°–60°N, 77.5°–122.5°E in Ding (1994); 45°–55°N, 90°–105°E in Wu and Chan (1997)]. As shown in Fig. 7, both USB and the Siberian high intensify before day 0 and weaken after day 2. When the Siberian high intensifies, the SAT over it drops, and vice versa. In addition, the pressure gradient force over the midlatitudes in East Asia is enhanced during the development of USB. The central SLP of the Siberian high increases from 1,036 hPa on day −2 (Fig. 4c) to over 1,040 hPa on day 0 (Fig. 5c). Apart from substantial cooling over the southeast quadrant of the cold high, the zonal pressure gradient tightens due to a drop in pressure over the Far East (i.e., downstream of the USB). As suggested by Takaya and Nakamura (2005a), the cold SAT anomalies over western Siberia induce upper-level cyclonic vorticities and low-level anticyclonic anomalies, which tend to maintain the upstream blocking and to construct quasi-stationary cyclonic anomalies over East Asia (see their Fig. 8b). Therefore, USB is believed to exert an impact on EAWM activities, which will be discussed in Sect. 5.3.

4 Characteristics of strong and weak USB events

In Sect. 3, the physical structure of a USB event throughout its life cycle and the impact of USB on EAWM activities were studied from the climatological point of view. However, each blocking event is unique, with different intensities, extensions, and durations. We are curious about the physical mechanisms responsible for these different USB characteristics. A recent study by Cheung et al. (2012b) sampled all Northern Hemisphere blocking events and showed that these characteristics are positively correlated with each other at the 95 % confidence level. Table 2 summarizes the linear correlation coefficients among these characteristics for 68 wintertime USB events. Findings are

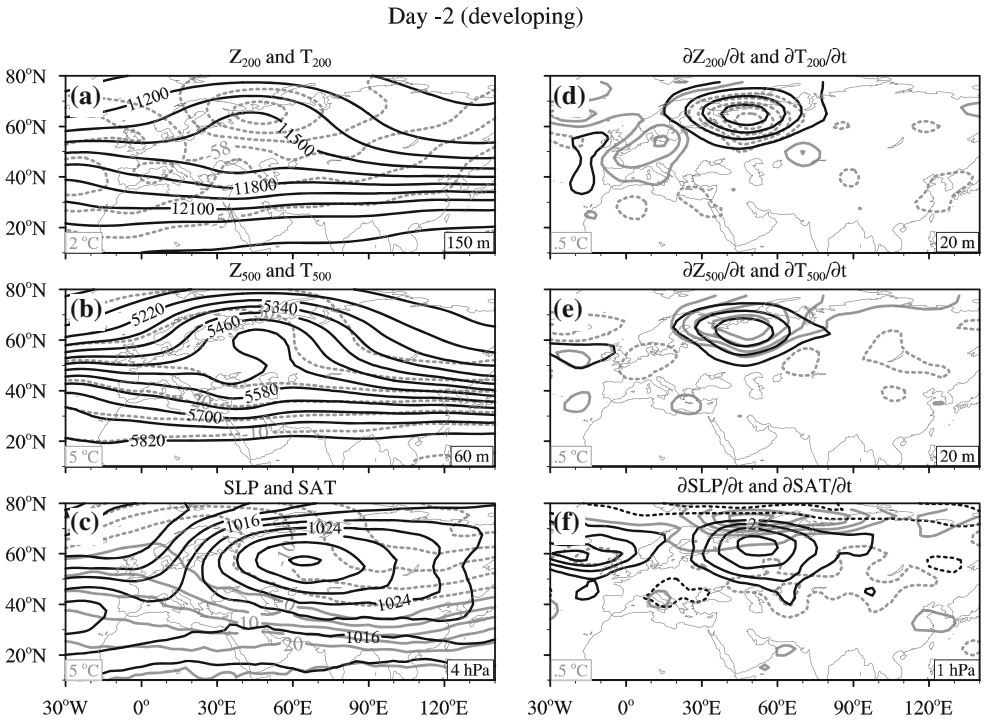

Fig. 4 (*Left panel*) **a**–**b**: Composite maps of geopotential height and air temperature at **a** 200 hPa and **b** 500 hPa; **c** sea level pressure (SLP) and surface air temperature (SAT) on day −2. (*Right panel*) **d**–**f**: Tendency of the quantities (i.e., day −2 minus day −3) in (**a**–**c**). The *black* contours indicate the geopotential height and SLP, whereas the *gray* contours indicate temperature. The contour interval of geopotential height and SLP is given at the *bottom right* of the composite and that of temperature is given at the *bottom left*

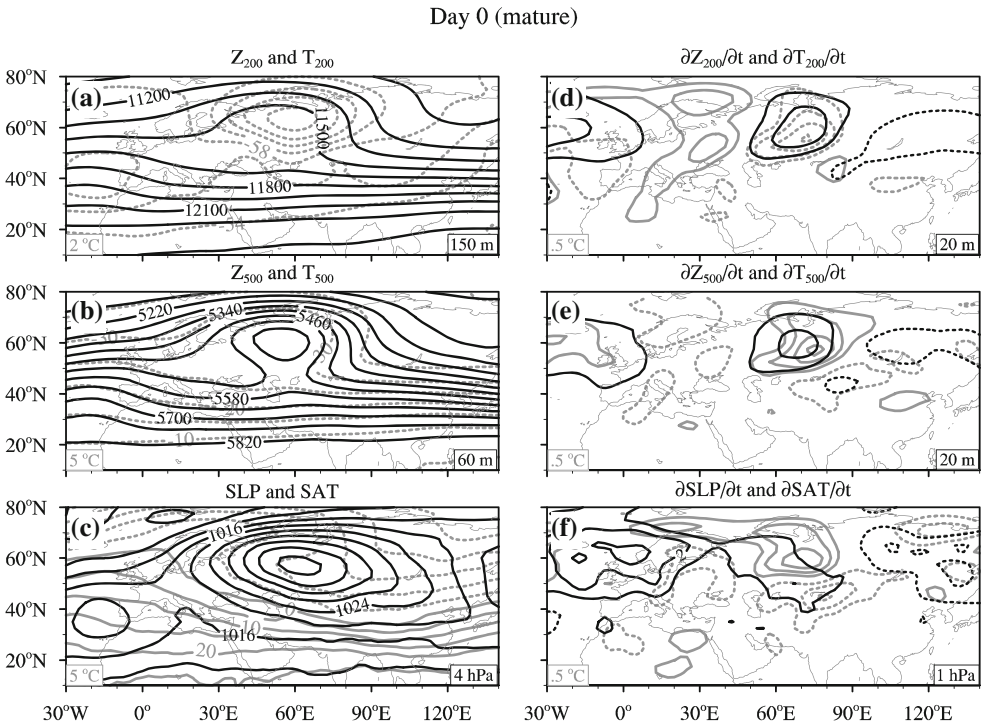

Fig. 5 Same as Fig. 4, but for day 0

similar to those of Cheung et al. (2012b) in that the correlation is particularly strong between the intensity and extension, with an explained variance of nearly 45 %. In comparison, the correlations between the duration and the other two characteristics account for less than 10 % of the total variance, despite the fact that the two correlation coefficients exceed the 90 % confidence level. Therefore, it is reasonable to assume that blocking events of high intensity and large extension share common features, and vice versa. The following analysis will focus only on the intensity of USB events. Due to the high interrelationship of intensity with extension, we classify the 68 events into three categories: strong, normal, and weak. Strong (weak) events are those with intensities greater (smaller) than the

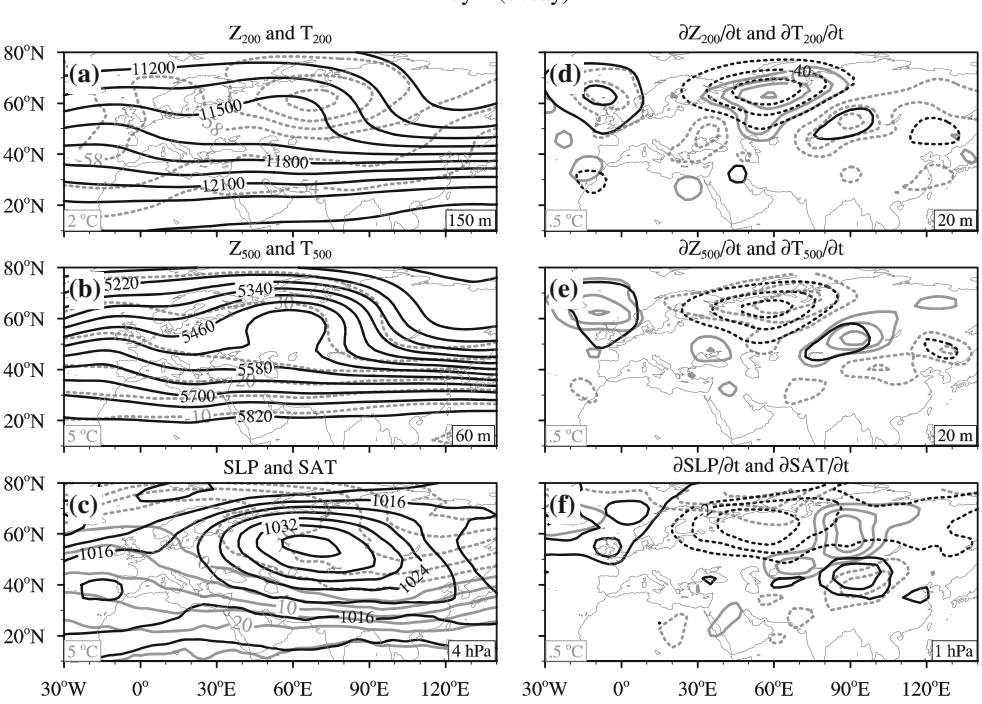

Fig. 6 Same as Fig. 4, but for day 2

75th (25th) percentile of intensity listed in Table 1, and the others are designated as normal events. The means of intensity, extension, and duration for strong/weak events are 7.01/2.07 (dimensionless), 2,440/1,200 km, and 7/4 days, respectively.

In Sect. 3.2, it was suggested that horizontal advection plays a dominant role in the development and decay of USB events (Figs. 4, 6). In addition, Sect. 3.1 illustrated that the height structure is pronounced throughout the entire air column and the warm-core structure is confined to the troposphere. In order to identify the precursor and impact of USB of different intensities, the intensity of 68 USB events is first regressed onto the thickness height tendencies and height anomalies in the 1,000–100 hPa layer, as well as the thickness air temperature anomalies in the 1,000–300 hPa layer, with different time lags. These regression maps are shown in Fig. 8, and the following describes the results for the characteristics of strong and weak events.

4.1 Physical forcing across the USB center

As mentioned in Sect. 3.1, a USB event is characterized by a mature omega-like spatial structure on day 0, with warm and high anomalies spreading across the Ural-Siberian region. Accordingly, the regression map on day 0 implies that a strong USB event is composed of a center of warmer and higher anomalies (Fig. 8h, m). It is questionable whether the development of such a structure is related to stronger physical forcing.

Table 3 (Table 4) summarizes the magnitude of the terms in the 1,000–300 hPa (1,000–100 hPa) layer in the temperature (vorticity) tendency equation (Eqs. 3–4) for the strong and weak events from day −2 to day 0. Generally, horizontal advections make the most significant contribution to the development of the two groups. In comparison, the thickness temperature and height anomalies between the two groups are remarkably different, that is, well above the 99 % confidence level. However, the difference is not as great for most of the other terms. For the temperature tendency equation, the confidence level is close to 90 % for the thickness temperature tendency and horizontal temperature advection. Furthermore, the magnitude of the adiabatic and diabatic terms diverges among the events of each group, whereas the difference in the two terms between the two groups is insignificantly small. For the vorticity tendency equation, even though the horizontal vorticity advection of the strong events is stronger than the weak events near the 95 % confidence level, this group is subject to a much stronger ageostrophic vorticity tendency. As a consequence, the Laplacian of geopotential height is significant only at the 90 % confidence level. In the decay stage, the differences in temperature and height anomalies between the two groups are still significant at the 99 % level, which is higher than the other terms (not shown). It appears that the difference in both dynamic and thermodynamic forcing cannot fully explain the discrepancy in the USB structures with different intensities. Thus, we attempt to identify the precursors for the strong and weak events.

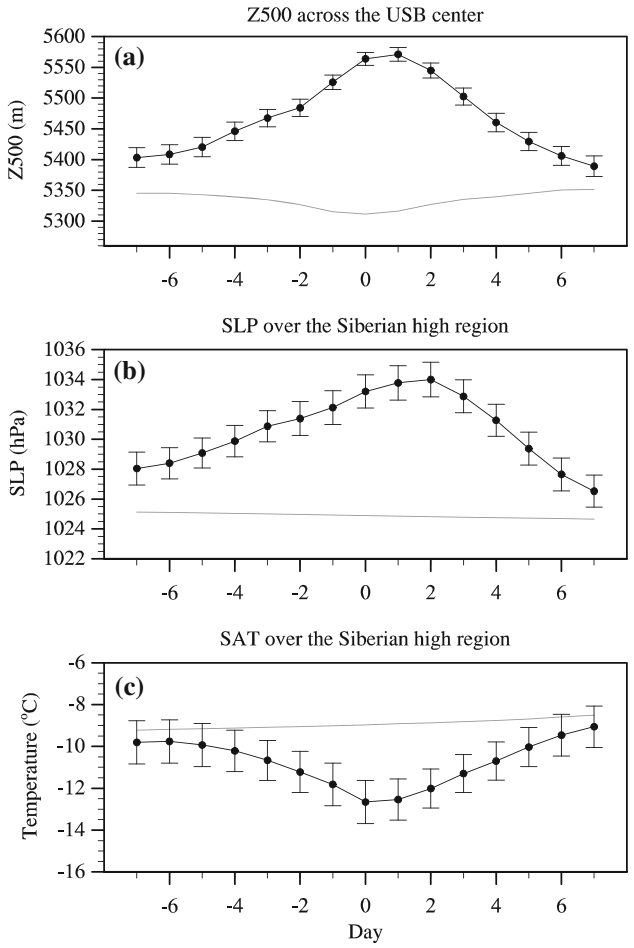

Fig. 7 **a** Z500 spanning 5° across the USB center; **b** SLP and **c** SAT over the Siberian high region (45°–55°N, 70°–90°E) from day −7 to day 7 (*black line*), where the climatological mean is represented by the *gray line* and the standard error of each quantity on each day is represented by the *error bar*

4.2 Amplified ridge over Europe

Nakamura et al. (1997) and Takaya and Nakamura (2005b) pinpointed that blocking over Eurasia is manifested mainly by an eastward-propagating quasi-stationary Rossby wavetrain from the Euro-Atlantic region. Both studies also concluded that transient eddy forcing associated with storm activities is of secondary importance in the development of blocking over this sector. As depicted in Fig. 9, a trough deepens over the North Atlantic and a ridge extends northeastward from Europe at the 500-hPa level on day −4 and day −3 for the strong events (Fig. 9a, c), but this is not apparent for the weak events (Fig. 9b, d). Correspondingly, there was already a sharp contrast in height and temperature anomalies between the two groups before the USB development between day −3 and day 0. This partly explains the marked difference in these two quantities compared to other physical forcing terms in Tables 3 and 4. This also suggests that the strong events are characterized by stronger amplification of a Rossby wavetrain. Indeed, Tyrlis and Hoskins (2008b) found the preexisting ridge over Europe to be a characteristic of wintertime Asian blocking.

4.3 Cyclogenesis over the Mediterranean Sea

From day −3 to day −1, a region with negative regression coefficients of thickness height tendencies moves southeastward from the European continent toward the Mediterranean Sea (Fig. 8a–b), where the coefficients are of the same sign at different levels (not shown). Meanwhile, another region with positive coefficients of this tendency term is expanding over Ural–Siberia. By comparing the magnitude of this tendency term to that in Fig. 4f, it can be deduced that the regression pattern indicates a cyclogenesis is taking place upstream of a developing USB event. Indeed, an explosive surface cyclogenesis was mentioned in earlier literature as being important for the formation of blocking (Colucci 1985; Tsou and Smith 1990). Specifically, Lupo and Smith (1995a) found that its occurrence frequency is highest in winter and lowest in summer. Furthermore, they obtained a statistically significant relationship between the deepening rate of a cyclone and the intensity of blocking over Atlantic and Pacific regions. The effect of cyclogenesis on the intensity of USB is noteworthy.

The composite maps shown in Fig. 10 compare strong and weak USB events. On day −1, the developing USB of both groups is observed to undergo the strongest intensification near the high anomaly center (Fig. 10a–d). Obviously, the positive temperature and height tendencies of the strong events are much higher than those of the weak events (Fig. 10e–f). Moreover, the cyclogenesis for the strong events is likely to occur over the Mediterranean Sea (Fig. 10a), while that for the weak events is not clear (Fig. 10b). In addition to a negative regression coefficient over this region of the thickness height anomalies on day 0 (Fig. 8g), it is suspected that the strength of cyclogenesis upstream of a USB event can potentially contribute to its intensity.

4.4 Surface cold anomalies over western Siberia

Apart from surface cyclogenesis, surface cold anomalies over the Siberian high can also induce surface anticyclonic vorticity anomalies over Ural–Siberia (Takaya and Nakamura 2005a). On day −3, positive regression coefficients of the thickness temperature anomaly in the 1,000–300 hPa layer can be identified over Siberia (60°–70°N, 60°–100°E; Fig. 8k). This is reflected by above-normal (below-normal) SATs over this region for the strong (weak) events, as implied

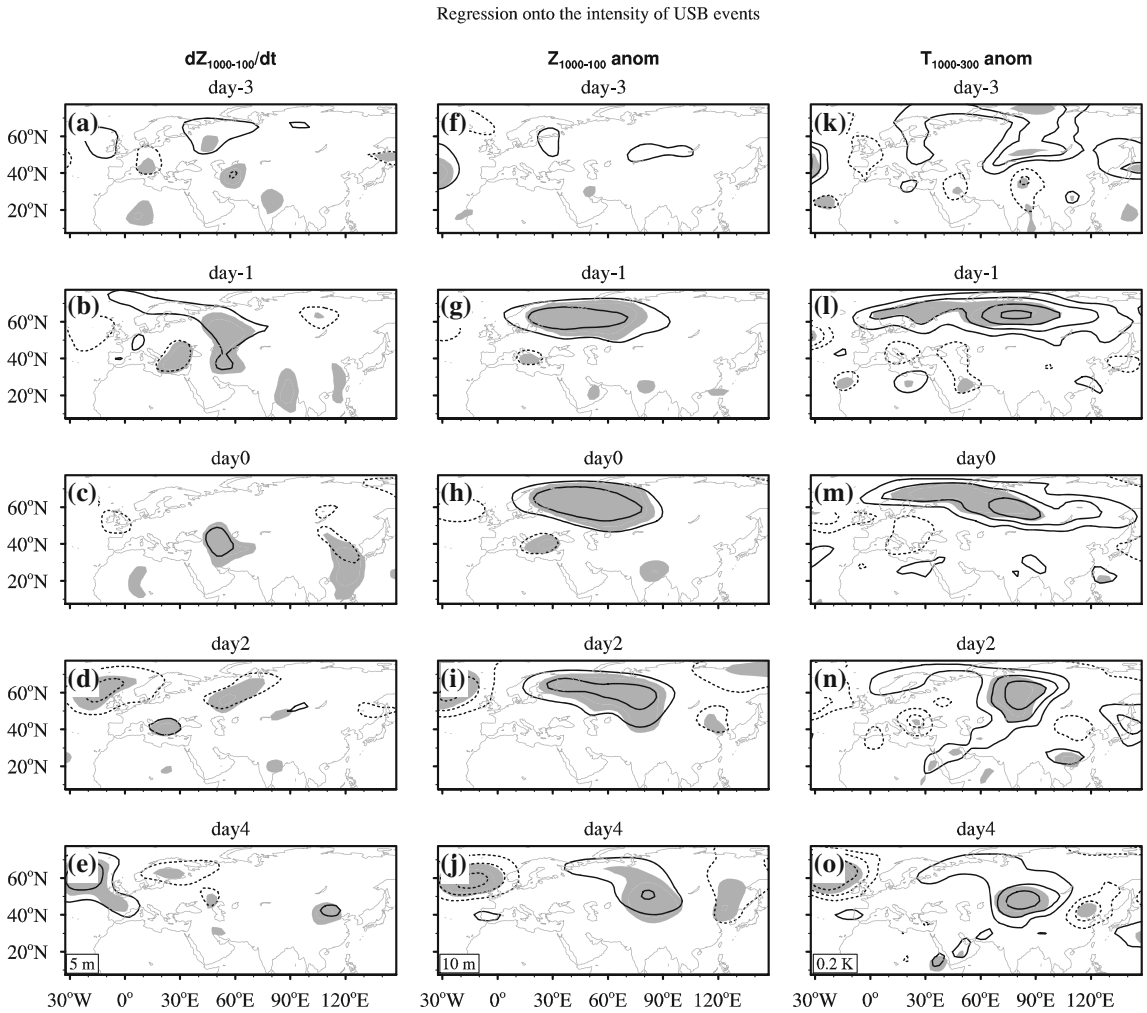

Fig. 8 Regression of the intensity of USB events onto the *thickness* height tendencies in the 1,000–100 hPa layer (*left panel*), height anomalies in the 1,000–100 hPa layer (*middle panel*) and temperature anomalies in the 1,000–300 hPa layer (*right panel*) on day −2, −1, 0, 2, and 4. The contour interval is indicated at the *bottom left* of the *bottom panel*. The zero values are omitted and negative values are *dashed*. The *shading* indicates that the regression coefficients are statistically significant at the 95 % confidence level

Table 2 Pearson's correlation matrix for the temporal characteristics of wintertime USB events, where the level of confidence is shown inside the brackets

Correlation	Intensity	Extension	Duration
Intensity		0.670 (>99.9 %)	0.262 (96.9 %)
Extension	0.670 (>99.9 %)		0.233 (94.4 %)
Duration	0.262 (96.9 %)	0.233 (94.4 %)	

by Fig. 11a–b. In addition, the two groups consist of a dipole temperature anomaly pattern during their development, in which the axis along the warm–cold anomaly center for the strong (weak) events is oriented in an N–S (NW–SE) direction (Fig. 11a–b). On one hand, a warm anomaly region spreading over the high latitudes during the strong events favors their large extension (Fig. 11a). On the other hand, the preexisting cold anomalies over the high latitudes of Siberia may play a key role in the development of the weak events (Fig. 11b). That is, this precursor indirectly enhances anticyclonic and warm eddies imported from upstream, which may be favorable for USB formation without upstream cyclogenesis. The next section discusses the impact of strong and weak events on EAWM activities.

4.5 Evolution of the Siberian high

Over the Siberian high region (45°–55°N, 70°–90°E on the transformed grid), both the SLP and SAT anomalies are comparable between the strong and weak events before USB formation (Fig. 12b–c). After USB formation, the SLP anomaly of strong events is slightly higher than that of weak events (Fig. 12b), but the SAT anomaly of weak events is lower than that of strong events around day 2

Table 3 Mean and standard error of temperature anomalies and each of the terms in the temperature equation for strong and weak USB events, as well as the difference between the two groups, in the 1,000–300 hPa layer averaged from day −2 to day 0

Term	Strong	Weak	Strong–weak (confidence level)
Day −2–0			
Temperature anomaly (°C)	7.25 ± 0.19	4.00 ± 0.51	3.25 (>99.9 %)
Temperature tendency (°C day^{-1})	1.93 ± 0.38	1.00 ± 0.36	0.924 (91.3 %)
Horizontal temperature advection (°C day^{-1})	3.13 ± 0.49	1.95 ± 0.52	1.18 (89.3 %)
Adiabatic heating (°C day^{-1})	0.603 ± 1.242	0.599 ± 1.001	0.00440 (0.22 %)
Diabatic heating (°C day^{-1})	0.435 ± 0.961	0.197 ± 0.962	0.238 (13.8 %)

The confidence level for the difference in each term is determined by the 2-tailed Student's *t* test and is shown inside the brackets

Table 4 Mean and standard error of geopotential height anomalies and each of the terms in the vorticity equation for strong and weak USB events, as well as the difference between the two groups, in the 1,000–100 hPa layer averaged from day −2 to day 0

Term	Strong	Weak	Strong–weak (confidence level)
Day −2–0			
Height anomaly (m)	275 ± 14	187 ± 17	87.6 (>99.9 %)
Laplacian of height tendency (10^{-10} s^{-2})	−0.802 ± 0.100	−0.459 ± 0.165	−0.342 (91.4 %)
Horizontal vorticity advection (10^{-10} s^{-2})	−1.39 ± 0.19	−0.82 ± 0.21	−0.571 (94.6 %)
Ageostrophic vorticity tendency (10^{-10} s^{-2})	0.200 ± 0.034	0.0335 ± 0.0318	0.1663 (99.9 %)
Vorticity divergence (10^{-10} s^{-2})	0.245 ± 0.082	0.109 ± 0.068	0.209 (79.2 %)

The confidence level for the difference in each term is determined by the 2-tailed Student's *t* test and is shown inside the brackets

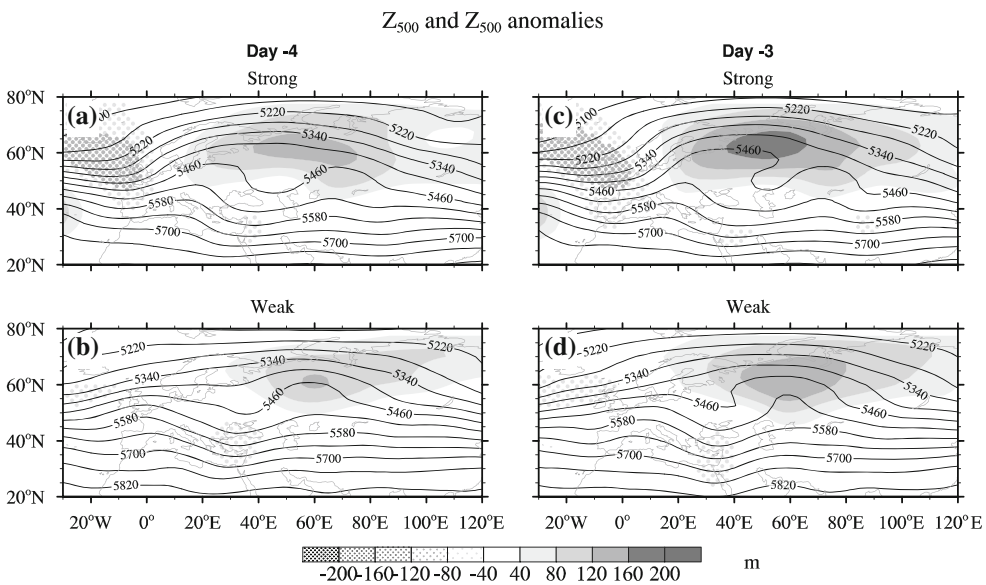

Fig. 9 Lagged composites of Z500 (*contour*) and Z500 anomalies (*shading*) for strong and weak USB events **a–b** day −4 and **c–d** day −3. The contour interval is 60 m

(Fig. 12c). The contrast between these two quantities of the strong and weak events may arise from their different precursors. The upstream environment of the strong events, which includes a cyclogenesis and a preexisting ridge, is essential for stronger amplification of the Siberian high. For the weak events, the preexisting cold anomalies over the high-latitude region of Siberia potentially enhance the intensity of cold air over the Siberian high region. From day 0 to day 4, USB tends to moves eastward slowly and a low is likely to develop over northeastern China and in the vicinity of Japan (Fig. 8h–j). As mentioned previously, a stronger USB event is associated with a stronger amplification of the Rossby wavetrain. Even though the cold anomalies over the Siberian high during the strong events

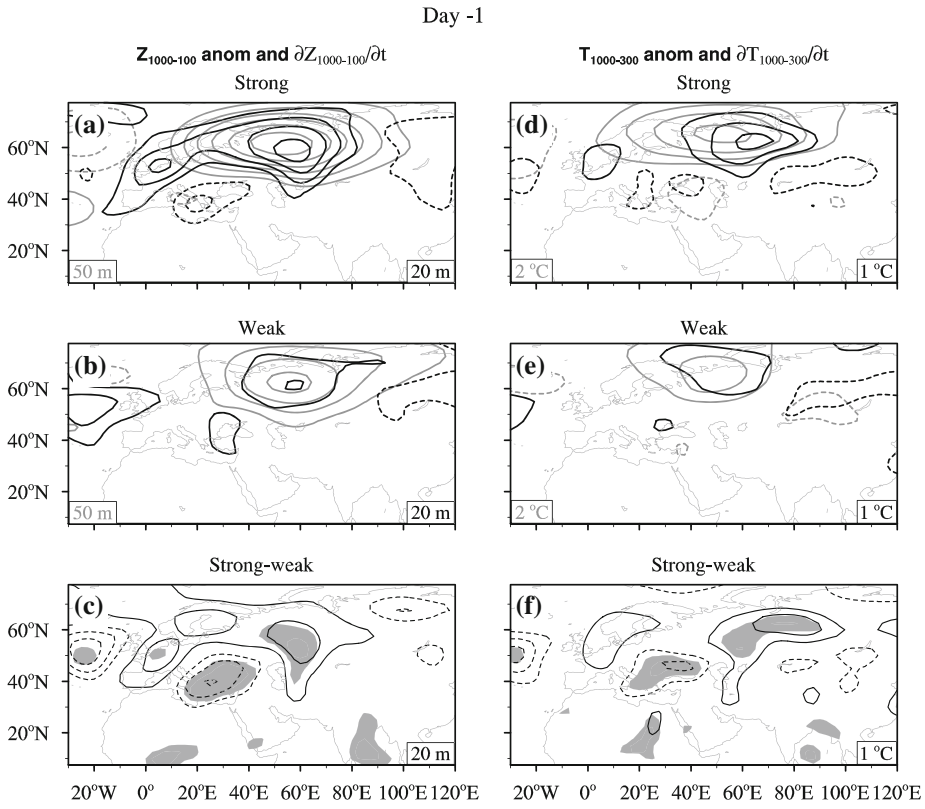

Fig. 10 *Upper* and *middle* panels show the thickness structure and forcing of **a–b** height in the 1,000–100 hPa layer and **d–e** air temperature in the 1,000–300 hPa layer for strong and weak USB events on day −1, where the tendencies and anomalies are represented by the *black* and *gray* contours, respectively. The *bottom panel* shows the difference in (**c**) thickness height tendencies and **f** thickness air temperature tendencies between strong and weak events, where the shading exceeds the 95 % confidence level based on the two-tailed Student's *t* test. The contour interval for *black* (*gray*) contours is shown at *bottom right* (*left*), where the zero contours are omitted and the negative contours are *dashed*

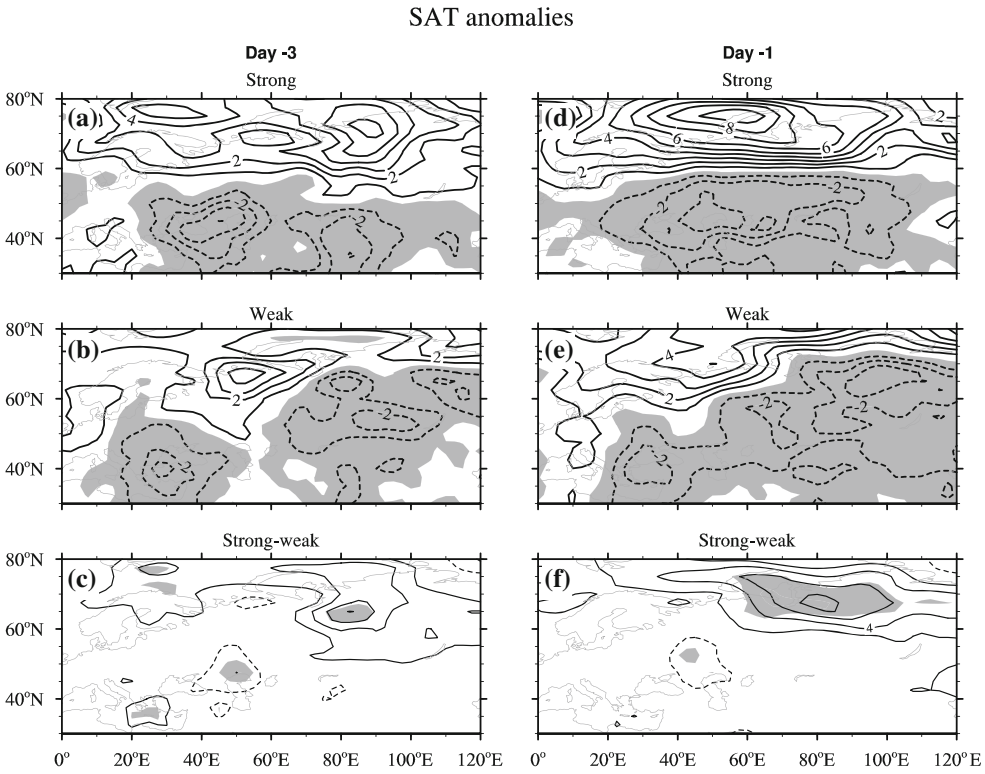

Fig. 11 *Upper* and *middle* panels show the surface air temperature anomalies for strong and weak USB events, whereas the *bottom panel* indicates the difference between the two groups on day −3 (*left panel*) and day −1 (*right panel*). The contour interval is 1.0 °C, where the zero contours are omitted and the negative contours are *dashed*. Negative values in the *upper* and *middle panels* and the differences exceeding the 95 % confidence level in the *bottom panel* are *shaded*

may be smaller in magnitude than during the weak events, an intense cooling is evident from day 4 to day 6, as inferred from Fig. 13a, c. This may be related to physical processes involved in the intensification of the Siberian high associated with the strong events, such as stronger northerly cold advection in the low levels. However, the

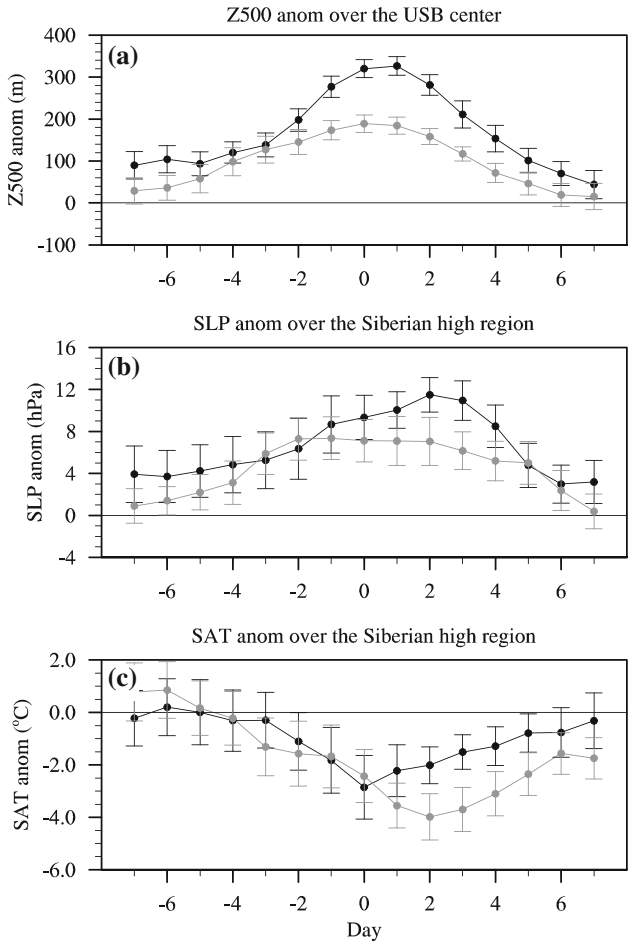

Fig. 12 **a** Z500 anomalies spanning 5° across the USB center; **b** SLP anomalies and **c** SAT anomalies over the Siberian high region (45°–55°N, 70°–90°E) for strong (*black lines*) and weak (*gray lines*) USB events from day −7 to day 7, where the standard error of each quantity on each day is represented by the *error bar*

detailed analyses of cold surges are beyond the scope of the present study. In short, the impact of both strong and weak USB events on EAWM activities is apparent.

5 Summary and discussion

5.1 Physical mechanisms of USB

The physical mechanisms and characteristics of Ural-Siberian blocking (USB) are investigated for the period 1980/1981–2009/2010. The climatological structure of a USB event is an omega-like spatial pattern in the upper levels. Its center is a warm core in the troposphere and a cold core in the lower stratosphere. Its development is attributed mainly to horizontal temperature and vorticity advections, which can be achieved by two pathways. The first one is initiated by an upstream cyclogenesis over the Mediterranean Sea, together with a ridge extending northeastward and undergoing amplification from Europe. This mechanism is similar to what was proposed by Lupo (1997), where blocking was observed to form in a high-amplitude planetary-scale flow regime due to advections of synoptic-scale eddies from a surface cyclone. This pathway is favored by an eastward shift of the climatological storm track over the North Atlantic toward the Mediterranean Sea, which is related to the North Atlantic Oscillation (Shabbar et al. 2001; Scherrer et al. 2006; Luo et al. 2010).

The second pathway is induced by cold SAT anomalies over Siberia. As suggested by Takaya and Nakamura (2005a), the cold Siberian high would interact with an upper-tropospheric Rossby wave. Specifically, it induces anomalous southwesterly and anticyclonic vorticity advections upstream, which allows an upstream ridge to form and remain quasi-stationary over Ural–Siberia. According to the postulation of Shabbar et al. (2001), the strong thermal contrast over the Euro-Atlantic region arising from a warm ocean–cold continent would echo the topographic forcing that favors blocking development over that region. In an analogous situation, warm SAT anomalies upstream of cold SAT anomalies over Siberia can trigger a USB event via the topographic forcing of the Ural Mountains. Therefore, the development of USB is initiated mainly by surface forcing.

Without the support of the above forcing, a USB event tends to weaken. We found that the adiabatic and diabatic terms become strong along the vertical structure after the mature stage of USB, but they tend to counteract each other. The diabatic cooling and the horizontal warm advection in the lower stratosphere tend to destroy the thermal structure of a USB event. In addition, cyclonic vorticity advection destroys the anticyclonic structure of a USB event. Overall, the baroclinic processes of horizontal advections are of utmost importance in the climatological life cycle of a USB event. Other terms, such as adiabatic warming and tilting, seem to play an insignificant role.

5.2 Relationship between intensity and extension

There is a strong statistical linkage between the intensity and extension of USB events, which can be explained by the physical mechanisms discussed above. By studying USB events of high and low intensity (which are called strong and weak), we noticed that the former (latter) group is likely to develop via the first (second) pathway. In comparison, the strong events are supported by the stronger physical forcing associated with cyclogenesis, which supplies plentiful warm subtropical air along the high latitudes over Siberia. Due to the absence of cyclogenesis, the warm anomalies of the weak events are more localized upstream of the developing USB. This emphasizes the role of

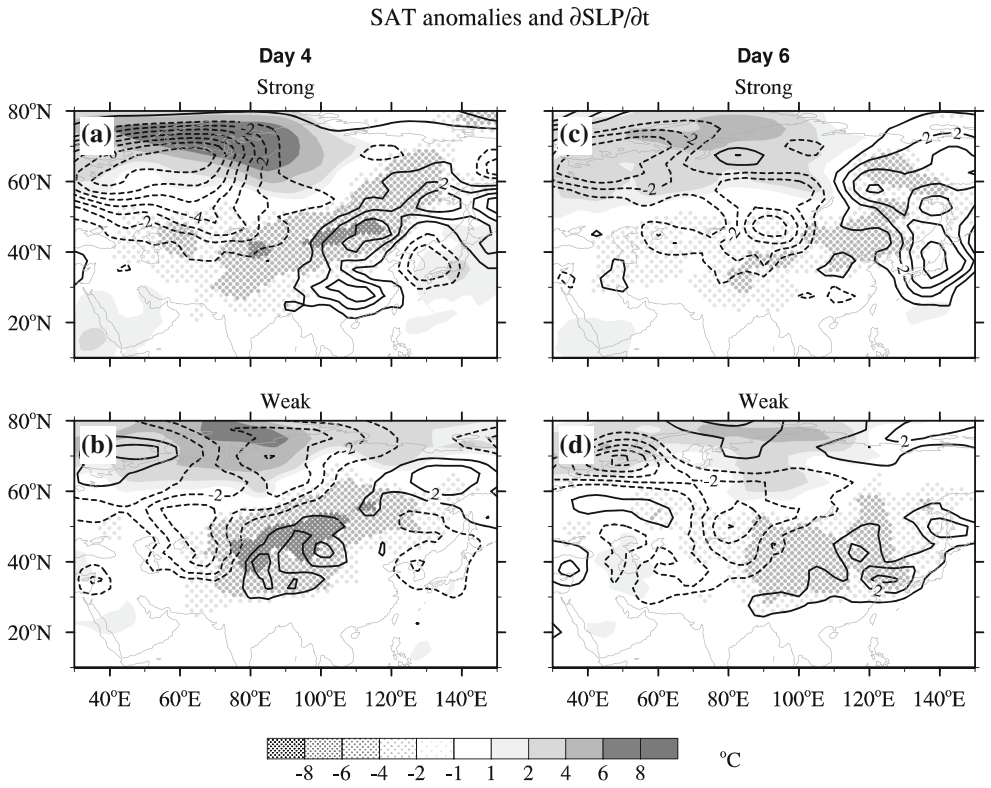

Fig. 13 SAT anomalies (*shading*) and tendency of SLP (*contour*) for strong and weak USB events on **a–b** day 4 and **c–d** day 6. The contour interval is 1 hPa, where the zero contours are omitted and the negative contours are *dashed*

cyclogenesis in the intensity and extension of a USB event. Indeed, Lupo and Smith (1995a) also mentioned this factor as the cause of the difference in these temporal features between summertime and wintertime blocking.

5.3 The impact of USB on EAWM activities

The physical mechanisms of USB events with different characteristics are important for understanding the relationship between USB and EAWM activities. Since the formation of weak USB events is preceded by cold SAT anomalies over western Siberia, these have an implicit linkage with the Siberian high. On the other hand, in strong events the upstream cyclogenesis over the Mediterranean Sea advects warm eddies poleward via a warm ridge. Meanwhile, the warm ridge also amplifies a thermal trough to advect cold polar air equatorward and downstream. Because the downstream side is usually the climatological Siberian high region, a dynamic linkage is established between strong USB events and the Siberian high.

In this study, we also found that the life cycle of a USB event is closely related to the evolution of the Siberian high. Recall that the Siberian high is a semipermanent feature of the EAWM. The anticyclonic flow diverging equatorward from the Siberian high consists of two branches, one traveling eastward toward the central Pacific and the other traveling southward and crossing the Maritime continent (Lau and Li 1984; Ding and Krishnamurti 1987; Ding 1994; Zhang et al. 1997; Chang et al. 2006). Zhou et al. (2007a, b) identified north–south and east–west SLP gradients as two leading spatial patterns over the EAWM. Particularly, they used the second mode as a measure of EAWM activities. During the formation of USB, cold SAT anomalies over the Siberian high interact with the quasi-stationary Rossby wave aloft (Takaya and Nakamura 2005a). Cyclonic anomalies are induced over East Asia, such that the pressure drops and the zonal pressure gradient tightens. Hence, USB is able to enhance EAWM activities.

Indeed, the circulation pattern associated with USB shares some common features with a typical cold surge. The Siberian high is developed under radiative cooling and the subsidence of cold air masses converging toward an approaching upper tropospheric trough (Ding 1990; Wu and Chan 1997). When the cold high touches the northeastern tip of the Tibetan Plateau, a cold surge is initiated (Hsu 1987). During a cold surge period, a ridge often occurs upstream of the trough (Chu 1978), such that an inverse phase relationship can be identified between Central Asia and East Asia (Chang and Lau 1980). Such a phase relationship is also present for the omega-like pattern of USB, but this can be long-lasting due to the persistence of USB. The persistence of USB maintains the cyclonic

vorticity downstream, which favors the accumulation of cold air over the Siberian high. Once the cold dome moves toward the lee side of the Tibetan Plateau, a cold air outbreak takes place and spreads across East Asia. Therefore, the recurrence of USB can lead to a long-lasting cold period in the EAWM, such as that of January 2008 (e.g., Zhou et al. 2009). Moreover, when the quasi-stationary trough propagates eastward in the decay stage of USB, a severe cold surge is likely to occur.

6 Concluding remarks

We have revealed that horizontal advections of temperature and vorticity are crucial for the development and decay of USB. There are two triggering mechanisms, which are (1) an upstream cyclogenesis over the Mediterranean Sea, and (2) surface cold anomalies over western Siberia. When only the former (latter) factor exists, USB is likely to be more (less) intense and extensive. Nevertheless, both pathways enhance EAWM activities. This highlights the importance of studying the physical linkage between blocking and EAWM activities on subseasonal timescales. A recent study by Chang and Lu (2012) demonstrated the possible impact of Pacific blocking on intraseasonal variations in the EAWM during the positive phase of Arctic Oscillation. On the other hand, Cheung et al. (2012a) proposed a combined effect of the Arctic Oscillation and El Niño/Southern Oscillation on the relationship between USB and the EAWM. We may consider how the intraseasonal oscillations of large-scale teleconnection patterns may impact USB and its temporal characteristics. The prediction limit of daily 500-hPa geopotential height (which is used for identifying blocking in this study) is around 6–11 days over the extratropics (Li and Ding 2011), which is shorter than the predictability over the tropics (Ding et al. 2011). Therefore, an advanced understanding of blocking can also improve the skill of extended-range weather forecasts.

Acknowledgments The first author was a recipient of a research studentship provided by the City University of Hong Kong. The work described in this paper was fully/partially supported by a grant from the Research Grants Council of the Hong Kong Special Administrative Region (Project No. 104410). The figures were prepared using the NCAR Command Language (Version 6.0.0). In addition, we appreciate the valuable comments and suggestions from the two anonymous reviewers.

References

Alberta TL, Colucci SJ, Davenport JC (1991) Rapid 500 mb cyclogenesis and anticyclogenesis. Mon Weather Rev 119: 1186–1204

Barriopedro D, Garcia-Herrera R, Lupo AR, Hernandez E (2006) A climatology of Northern hemisphere blocking. J Clim 19: 1042–1063

Blackmon ML, Lee YH, Wallace JM, Hsu HH (1984) Time variation of 500 mb height fluctuations with long, intermediate and short time scales as deduced from lag-correlation statistics. J Atmos Sci 41:981–991

Chan JCL, Li C (2004) The East Asia winter monsoon. In: Chang CP (ed) East Asian monsoon. World Scientific, Singapore, pp 54–106

Chang C-P, Lau KM (1980) Northeasterly cold surges and near-equatorial disturbances over the winter MONEX area during December 1974. II: Planetary-scale aspects. Mon Weather Rev 108:298–312

Chang C-P, Lu M–M (2012) Intraseasonal predictability of Siberian high and East Asian winter monsoon and its interdecadal variability. J Clim 25:1773–1778

Chang C-P, Wang Z, Hendon H (2006) The Asian winter monsoon. In: Wang B (ed) The Asian monsoon. Springer, Heidelberg, pp 89–128

Chen W, Li T (2007) Modulation of northern hemisphere wintertime stationary planetary wave activity: East Asian climate relationships by the Quasi-Biennial Oscillation. J Geophys Res 112: D20120. doi:10.1029/2007JD008611

Chen W, Yang S, Huang R (2005) Relationship between stationary planetary wave activity and the East Asian winter monsoon. J Geophys Res 110:D14110. doi:10.1029/2004JD005669

Cheung HN, Zhou W, Mok HY, Wu MC (2012a) Relationship between Ural-Siberian blocking and the East Asian winter monsoon in relation to the Arctic Oscillation and the El Niño-Southern Oscillation. J Clim 25:4242–4257

Cheung HN, Zhou W, Mok HY, Wu MC, Shao Y (2012b) Revisiting the climatology of atmospheric blocking in the Northern Hemisphere. Adv Atmos Sci. doi:10.1007/s00376-012-2006-y

Chu EWK (1978) A method for forecasting the arrival of cold surges in Hong Kong. Hong Kong Observatory Tech. Note. No. 43, p 31

Colucci SJ (1985) Explosive cyclogenesis and large-scale circulation changes: implications for atmospheric blocking. J Atmos Sci 42:2701–2717

Croci-Maspoli M, Schwierz C, Davies HC (2007) A multi-faceted climatology of atmospheric blocking and its recent linear trend. J Clim 20:633–649

Diao Y, Li J, Luo D (2006) A new blocking index and its application: blocking action in the northern hemisphere. J Clim 19:4819–4839

Ding Y (1990) Buildup, air-mass transformation and propagating of Siberian high and its relations to cold surge in East Asia. Meteor Atmos Phys 44:281–292

Ding Y (1994) Monsoons over China. Kluwer, Dordrecht

Ding Y, Krishnamurti TN (1987) Heat budget of the Siberian high and the winter monsoon. Mon Weather Rev 115:2428–2449

Ding R, Li J, Seo K (2011) Estimate of the predictability of boreal summer and winter intraseasonal oscillations from observations. Mon Weather Rev 139:2421–2438

Holopainen E, Fortelius C (1987) High-frequency transient eddies and blocking. J Atmos Sci 44:1632–1645

Holton JR (1979) An Introduction to dynamic meteorology. Academic, San Diego, p 391

Hsu H–H (1987) Propagation of low-level circulation features in the vicinity of mountain ranges. Mon Weather Rev 115:1864–1892

Illari L (1984) A diagnostic study of the potential vorticity in a warm blocking anticyclone. J Atoms Sci 41:3518–3526

Joung CH, Hitchman MH (1982) On the role of successive downstream development in East Asian polar air outbreaks. Mon Weather Rev 110:1224–1237

Kalnay E, Kanamitsu M, Kistler R, Collins W, Deaven D, Gandin L, Iredell M, Saha S, White G, Woolen J, Zhu Y, Leetmaa A, Reynolds R, Chelliah M, Ebisuzaki W, Higgins W, Janowiak J, Mo KC, Ropelewski C, Wang J, Jenne R, Joseph D (1996) The NCEP/NCAR 40-year reanalysis project. Bull Am Meteorol Soc 77:437–471

Lau KM, Li MT (1984) The monsoon of East Asia and its global associations—a survey. Bull Am Meteorol Soc 65:114–125

Li J, Ding R (2011) Temporal–spatial distribution of atmospheric predictability limit by local dynamical analogues. Mon Weather Rev 139:3265–3283

Li C, Gu W (2010) An analyzing study of the anomalous activity of blocking high over the Ural Mountains in January 2008. Chin J Atmos Sci 34(5):865–874 (In Chinese)

Lu M–M, Chang C-P (2009) Unusual late-season cold surges during the 2005 Asian winter monsoon: roles of Atlantic blocking and the Central Asian anticyclone. J Clim 22:5205–5217

Luo D, Zhou W, Wei K (2010) Dynamics of eddy-driven North Atlantic oscillations in a localized shifting jet: zonal structure and downstream blocking. Clim Dyn 34:73–100

Lupo AR (1997) A diagnosis of two blocking events that occurred simultaneously over the midlatitude Northern Hemisphere. Mon Weather Rev 125:1801–1823

Lupo AR, Smith PJ (1995a) Climatological features of blocking anticyclones in the northern hemisphere. Tellus 47A:439–456

Lupo AR, Smith PJ (1995b) Planetary and synoptic-scale interactions during the life cycle of a mid-latitude blocking anticyclone over the North Atlantic. Tellus 47A:575–596

Lupo AR, Smith PJ, Zwack P (1992) A diagnosis of the explosive development of two extratropical cyclones. Mon Weather Rev 120:1490–1523

Mullen SL (1987) Transient eddy forcing of blocking flows. J Atmos Sci 44:3–22

Nakamura H, Wallace JM (1993) Synoptic behavior of baroclinic eddies during the blocking onset. Mon Weather Rev 121:1892–1903

Nakamura H, Nakamura M, Anderson JL (1997) The role of high- and low-frequency dynamics in blocking formation. Mon Weather Rev 125:2074–2093

Pan H (1987) Winter-time 10–20 day variations in the upper troposphere. J Meteor Soc Jpn 65:587–603

Scherrer S, Croci-Maspoli M, Schwierz C, Appenzeller C (2006) Two-dimensional indices of atmospheric blocking and their statistical relationship with winter climate patterns in the Euro-Atlantic region. Int J Climatol 26:233–249

Shabbar A, Huang J, Higuchi K (2001) The relationship between the wintertime North Atlantic oscillation and blocking episodes in the North Atlantic. Int J Climatol 21:355–369

Takaya K, Nakamura H (2005a) Mechanisms of intraseasonal amplification of the cold Siberian high. J Atmos Sci 62:4423–4440

Takaya K, Nakamura H (2005b) Geographical dependence of upper-level blocking formation associated with intraseasonal amplification of the Siberian high. J Atmos Sci 62:4441–4449

Tao S (1957) A study of activities of cold airs in East Asian winter, handbook of short -term forecast (in Chinese), China Meteorological administration. Meteorology Press, Beijing, pp 60–92

Tao S, Wei J (2008) Severe snow and freezing rain in January 2008 in the southern China. Clim Environ Res 13(4):337–350 (in Chinese)

Tibaldi S, Molteni F (1990) On the operational predictability of blocking. Tellus 42A:343–365

Tracton MS (1990) Predictability and its relationship to scale interaction processes in blocking. Mon Weather Rev 118: 1666–1695

Trigo RM, Trigo IF, DaCamara CC, Osborn TJ (2004) Winter blocking episodes in the European-Atlantic sector: climate impacts and associated physical mechanisms in the reanalysis. Clim Dyn 23:17–28

Tsou C-H, Smith PJ (1990) The role of synoptic/planetary-scale interactions during the development of a blocking anticyclone. Tellus 42A:174–193

Tyrlis E, Hoskins BJ (2008a) Aspects of a northern hemisphere atmospheric blocking climatology. J Atmos Sci 65:1638–1652

Tyrlis E, Hoskins BJ (2008b) The morphology of northern hemisphere blocking. J Atmos Sci 65:1653–1665

Wang L, Chen W, Zhou W, Chan JCL, Barriopedro D, Huang R (2010) Effect of the climate shift around mid 1970s on the relationship between wintertime Ural blocking circulation and East Asian climate. Int J Climatol 30:135–158. doi:10.1002/joc.1876

Wu MC, Chan JCL (1997) Upper-level features associated with winter monsoon surges over South China. Mon Weather Rev 125:317–340

Wu MC, Leung WH (2009) Effect of ENSO on the Hong Kong winter season. Atmos Sci Lett 10:94–101

Zhang Y, Sperber KR, Boyle JS (1997) Climatology and interannual variation of East Asian winter monsoon: result from the 1979–95 NCEP/NCAR reanalysis. Mon Weather Rev 125:2605–2619

Zhou W, Li C, Wang X (2007a) Possible connection between Pacific oceanic interdecadal pathway and East Asian winter monsoon. Geophys Res Lett 34:L01701. doi:10.1029/2006GL027809

Zhou W, Wang X, Zhou TJ, Li C, Chan JCL (2007b) Interdecadal variability of the relationship between the East Asian winter monsoon and ENSO. Meteor Atmos Phys 98:283–293. doi:10.1007/s00703-007-0263-6

Zhou W, Chan JCL, Chen W, Ling J, Pinto JG, Shao Y (2009) Synoptic-scale controls of persistent low temperature and icy weather over southern China in January 2008. Mon Weather Rev 137:3978–3991